Journal of Medicinal Chemistry

Article

pubs.acs.org/jmc

Structural Basis of Selective Inhibition of Human Tankyrases†

Mohit Narwal, Harikanth Venkannagari, and Lari Lehtiö*

Pharmaceutical Sciences, Department of Biosciences, Abo Akademi University, FI-20520 Turku, Finland

Supporting Information

ABSTRACT: Tankyrases are poly(ADP-ribose) polymerases that have many cellular functions. They play pharmaceutically important roles, at least in telomere homeostasis and Wnt signaling, by covalently ADP-ribosylating target proteins and consequently regulating their functions. These features make tankyrases potential targets for treatment of cancer. We report here crystal structures of human tankyrase 2 catalytic fragment in complex with a byproduct, nicotinamide, and with selective inhibitors of tankyrases (IWR-1) and PARPs 1 and 2 (olaparib). Binding of these inhibitors to tankyrase 2 induces specific conformational changes. The crystal structures explain the selectivity of the inhibitors, reveal the flexibility of a substrate binding loop, and explain existing structure−activity relationship data. The first crystal structure of a PARP enzyme in complex with a potent inhibitor, IWR-1, that does not bind to the widely utilized nicotinamide-binding site makes the structure valuable for development of PARP inhibitors in general.

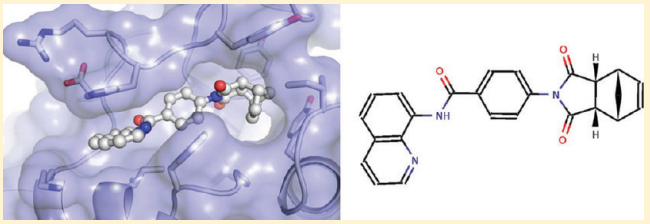

INTRODUCTION

Tankyrases belong to the poly(ADP ribose) polymerase (PARP) protein superfamily (EC 2.4.2.30). These multidomain proteins catalyze the transfer of ADP-ribose units from NAD^+ to the target protein one-by-one to form a polymer of ADP-ribose (pADPr). In the reaction, the NAD^+ molecule is cleaved to nicotinamide and an ADP-ribose electrophile, which is covalently attached to the target. This modification confers a large negative charge to the target protein and, hence, alters the interactive and functional properties thereof. PARPs are involved in many important cellular functions, such as detection and repair of DNA damage, regulation of transcription, intracellular trafficking, modification of chromatin, formation of the mitotic apparatus, and cell death.[1] The human PARP superfamily has 18 members, and according to the suggested new nomenclature, they are known as ADP-ribosyltransferases (ARTDs).[2] Human tankyrases 1 (TNKS1) and 2 (TNKS2) are members of this family and are also known as ARTD5 (PARP-5a) and ARTD6 (PARP-5b), respectively.

Tankyrases contain a HPS domain (present only in TNKS1), an ANK domain (24 ankyrin repeats), a SAM domain (sterile α motif), and an ART domain (ADP-ribosyltransferase). The HPS domain contains homopolymeric runs of histidine, proline, and serine and has an as-yet unknown function. The ANK domain is required for protein−protein interactions, whereas the SAM domain is responsible for the multimerization of tankyrase, which is also regulated by automodification.[3] The catalytic ART domain is common to all PARPs. TNKS1 and TNKS2 share 83% overall and 94% sequence identity for the ART domains. They have many overlapping functions, and they interact with a wide range of proteins.[4,5]

The tankyrases have gained attention as drug targets because of their roles in maintenance of the telomeres and in Wnt signaling. Inhibition of tankyrases has also been shown to induce selective lethality to BRCA-deficient cells,[8] and tankyrases also play an important role in assembly of the mitotic spindle.[6,7] These four functions make tankyrases attractive targets for cancer therapy. Tankyrases (TRF1 (telomere repeat binding factor) interacting ANKyrin-related ADP-ribose polymerases 1 and 2) interact with and modify TRF1. Poly(ADP-ribosyl)ation of TRF1 causes it to dissociate from telomeric DNA, leading to elongation of the telomers by a reverse transcriptase called telomerase. Long telomeres are typical for cancer cells,[9,10] and therefore, telomerase has been a target for drug development.[11] It has been shown that overexpression of TNKS1 leads to elongated telomeres,[12] and its inhibition enhances the effect of telomerase inhibitors.[13]

Tankyrases modulate Wnt signaling by modifying axin, a major component in the β-catenin destruction complex, for degradation. Extracellular Wnt signaling is often overactivated in cancers,[14,15] and inhibition of tankyrases counteracts the Wnt signal pathway by stimulating degradation of β-catenin.[16] Recently, potent inhibitors of Wnt signaling were discovered from high-throughput screens using a Wnt-responsive supertop flash luciferase reporter assay.[16,17] It was shown that the compounds affected Wnt signaling through the inhibition of tankyrases.[16] Here, we report the crystal structures of TNKS2 in complex with a byproduct (nicotinamide), a PARP1-selective inhibitor **1** (olaparib),[18] and a tankyrase-selective inhibitor **2** (IWR-1).[17] The potent and selective inhibitor **2** does not utilize the traditional nicotinamide-binding site occupied by most of the known PARP inhibitors. The loop lining the substrate-binding groove shows significant flexibility in order to accommodate inhibitors, and therefore, these structures will create new possibilities for structure-based drug design.

Received: November 8, 2011
Published: January 10, 2012

dx.doi.org/10.1021/jm201510p | J. Med. Chem. 2012, 55, 1360−1367

RESULTS

Overall Structure. The tankyrases and PARP1 share an ART domain that catalyzes ribosylation of target proteins and, in the case of tankyrase, the tankyrase protein itself (Figure 1).

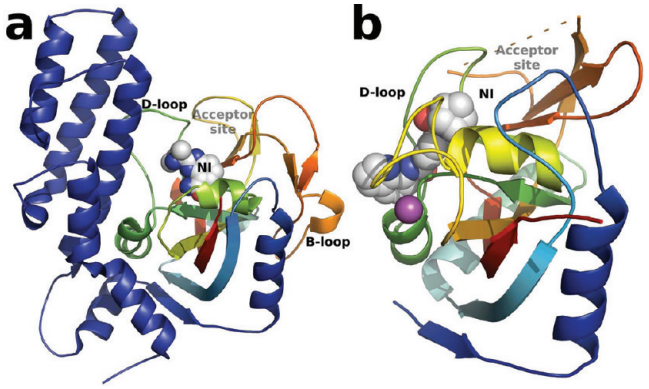

Figure 1. Overview of the crystal structure. Side-by-side comparison of (a) PARP1 and (b) TNKS2. Both structures are colored from the N-terminus (blue) to the C-terminus (red). The N-terminal regulatory domain of PARP1 is colored blue. The D-loop lining the donor NAD^+ binding cavity, B-loop of PARP1, nicotinamide-binding site (NI), and acceptor sites are labeled. The zinc ion of TNKS2 is shown as a sphere. Inhibitors **2** in TNKS2 and veliparib (ABT-888) in PARP1 (PDB code 2RD6[33]) are shown to indicate the inhibitor binding site.

PARP1 (like PARPs 1–4) also has an α-helical PARP regulatory domain (PRD) on the N-terminal side of the ART domain. The PRD domain closely interacts with the substrate-binding site and is thought to control branching of the pADPr chain.[19,20] On the "back side" of the ART domain, PARP1 contains a B-loop, which is not present in tankyrases (Figure 1). In the initiation reaction, NAD^+ is bound to the so-called donor site and cleaved and an ADP-ribose is added to the target protein bound to the acceptor site located between several loop structures (Figure 1). During the elongation reaction, the acceptor site is occupied by the growing polymer chain. The binding site of the donor NAD^+ and, especially, the nicotinamide-binding cleft have been utilized in the design of inhibitors (Figure 1). Comparison between PARP1 and tankyrases showed that the D-loop lining the donor site is three amino acid residues longer in PARP1 (Figure 1a).[21,22] Before crystallization, TNKS2 was cleaved with chymotrypsin; this causes a chain-break at a surface loop near the acceptor site (Figure 2). The ART domains of TNKS1 and TNKS2 are highly homologous, and all residues in the vicinity of the donor site are conserved.[22] The differences seen in the solved structures are mostly due to conformations of the flexible D-loop, as discussed below.

Nicotinamide-Binding Site. So far, no substrate-bound complexes of any PARP enzymes have been reported. In an attempt to obtain a substrate complex of TNKS2, we soaked crystals with high concentrations of NAD^+. Surprisingly, we observed that a byproduct, nicotinamide, instead of substrate was bound to the active site (Figure 2a). Nicotinamide is present in both molecules of the asymmetric unit but only with half-occupancy in monomer B. It binds as expected to the nicotinamide binding site of TNKS2 and forms interactions typical of nicotinamide-mimicking inhibitors: the carboxamide forms hydrogen bonds with the Ser1068 alcohol and with the main chain carbonyl and amide of Gly1032. Typical PARP

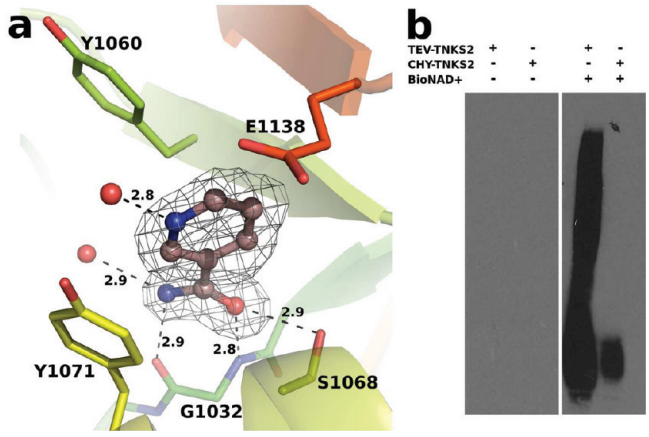

Figure 2. Nicotinamide-bound structure and activity assay. (a) Nicotinamide bound to the active site of TNKS2. The difference density observed before addition of nicotinamide to the model is shown as a mesh at 3σ. The structure is colored as in Figure 1b, and the distances are shown in Å. (b) Western blot showing the automodification activities of intact TNKS2 catalytic domain (TEV-TNKS2) and chymotrypsin-cleaved TNKS2 (CHY-TNKS2).

inhibitors form a $\pi-\pi$ stacking interaction with Tyr1071 (Tyr907 in PARP1). Nicotinamide does not effectively stack with the tyrosine, and the aromatic ring is at 39° from the tyrosine plane. Nicotinamide also forms hydrogen bonds with water-molecule networks close to the catalytic Glu1138 and His1031/Tyr1071 that form the conserved H-Y-E motif.[19] Because we observed a nicotinamide in crystals soaked with NAD^+, we tested whether the chymotrypsin-cleaved protein would be able to catalyze the ADP-ribosylation reaction. It was evident that the protein could indeed catalyze covalent automodification and not merely hydrolysis of NAD^+, although the activity was much lower than that of the uncleaved construct (Figure 2b).

Previously, **3** (XAV939) was reported as a inhibitor of selective tankyrases (IC_{50}(PARP1) = 2.2 μM, IC_{50}(PARP2) = 114 nM, IC_{50}(TNKS1) = 11 nM, IC_{50}(TNKS2) = 4 nM),[16] and recently, a complex structure of TNKS2 with **3** was reported.[21] It forms the same hydrogen bonds as does nicotinamide (Figure 3a): the pyrimidine N–H and carbonyl form hydrogen bonds with Ser1068 and Gly1032. The Tyr1071 side chain stacks with the pyrimidine ring of **3**. TNKS2 and **3** also have many nonpolar interactions, as the phenyl ring has interactions with the side chains of Tyr1050 and Tyr1071 and the trifluoromethyl group forms hydrophobic interactions with the Pro1034, Phe1035, and Ile1075 side chains (Figure 3a).[21] Notably, the structure of the protein was almost identical to the apo and to the nicotinamide-bound structure described here. There are only minor changes in the conformations of Phe1035, due to interaction with trifluoromethyl of **3**, and of Tyr1071, due to interactions at the nicotinamide site.

Binding of Olaparib. Olaparib **1** is a highly potent and selective inhibitor of PARP1 and PARP2 that is currently in clinical trials (IC_{50}(PARP1) = 5 nM, IC_{50}(PARP2) = 1 nM, IC_{50}(TNKS1) = 1.5 μM).[18,23] The complex with TNKS2 shows that binding induces a major conformational change of the D-loop residues (especially Asp1045, His1048, Ala1049, and Tyr1050). The His1048 blocking the cavity in previously reported apo and **3** complex structures moves out (Figure 3b). Indeed, the whole D-loop moves when **1** binds to TNKS2. At the nicotinamide-binding site, **1** forms similar hydrogen bonds

dx.doi.org/10.1021/jm201510p | J. Med. Chem. 2012, 55, 1360–1367

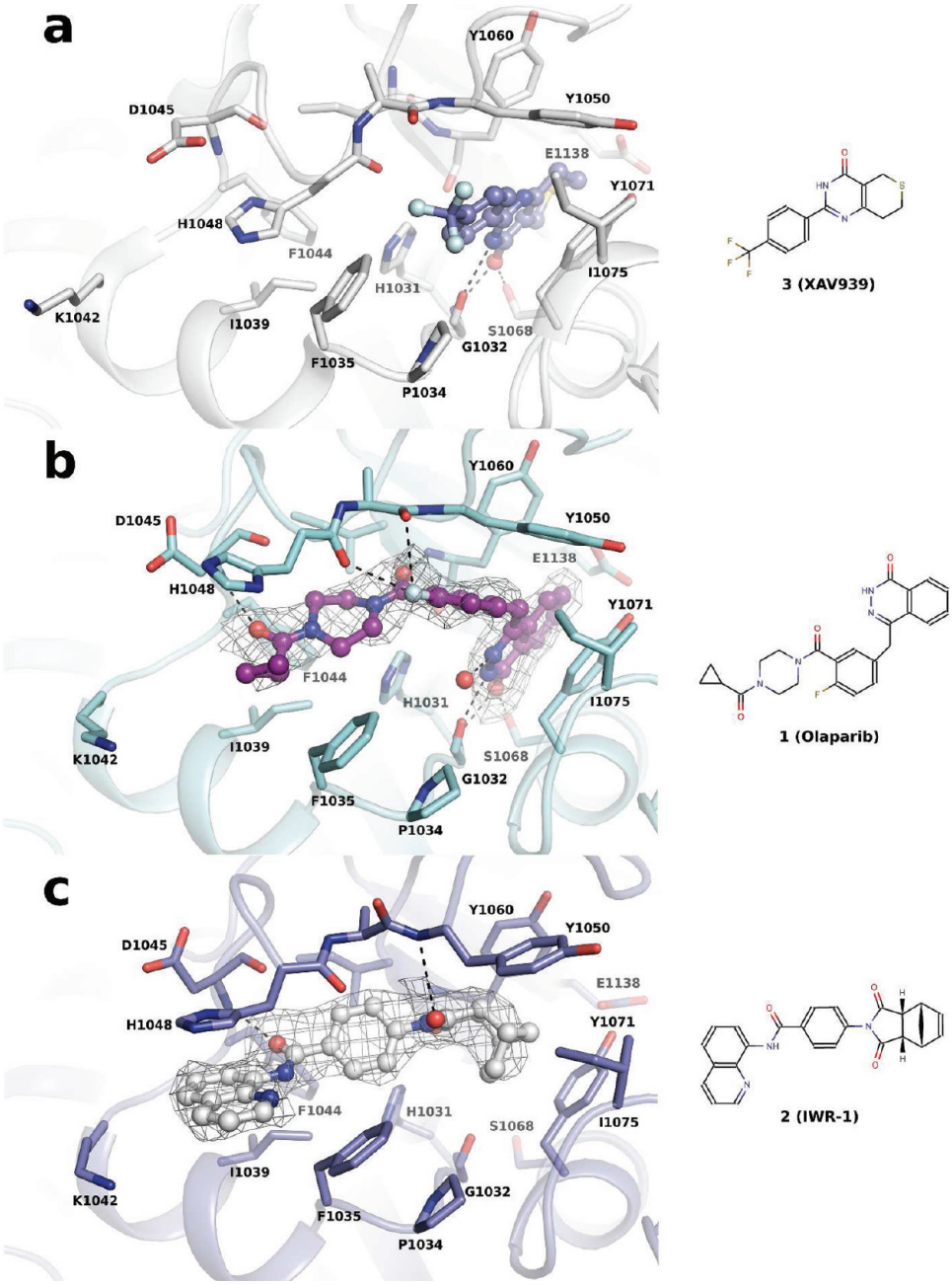

Figure 3. Comparison of TNKS2−inhibitor complexes. Identical views of the superposed structures of TNKS2 complexes of (a) **3** (PDB code 3KR8), (b) **1**, and (c) **2**. Corresponding residues surrounding the binding site are shown as sticks in each figure. For **1** and **2**, a difference density observed before addition of the compound is shown and contoured at 2σ.

with Ser1068 and Gly1032, as does nicotinamide and **3** (Figure 3b). The pyrimidine ring is parallel to Tyr1071 and forms an offset π-stacking interaction. It also forms a hydrogen bond with a water molecule bound to the carbonyl of Gly1032. The fluorophenyl group stacks with Tyr1050 of the D-loop. The fluorine of the fluorophenyl group interacts unfavorably with the D-loop, as the electronegative fluorine is within van der Waals distance from carbonyls of His1048 and Ala1049. The carbonyl groups of **1** form hydrogen bonds with the amides of Tyr1060 and Asp1045. The cyclopropyl interacts with the hydrophobic face of the helix 1035−1042 which lines the donor site. The binding can be divided so that interactions at the upper nicotinamide binding site follow the lock-and-key model, whereas at the lower end of the cavity, it follows the induced-fit mechanism.

Binding of IWR-1. The most remarkable and evident observation from the complex structure of TNKS2 and a potent inhibitor **2** (IC_{50}(TNKS1) = 131 nM, IC_{50}(TNKS2) = 56 nM)[16] is that **2** does not bind to the nicotinamide-binding site at all, unlike all the other PARP−inhibitor complex structures solved to date (Figure 1b). In addition, it induces a movement of the D-loop that is even larger than that observed with **1** (Figure 3c). The chemical structure of **2** can be divided into three parts: norbornyl, spacer, and amide regions (Figure 4). In the crystal structure, the carbonyl oxygens of the norbornyl region of **2** form three hydrogen bonds with protein main-chain atoms, two at the norbornyl part with the backbone amides of

dx.doi.org/10.1021/jm201510p | J. Med. Chem. 2012, 55, 1360−1367

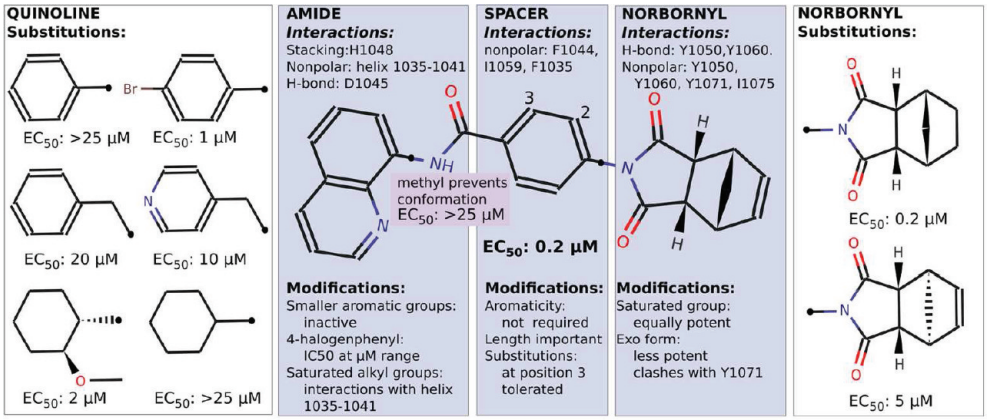

Figure 4. Structure of **2**. The structure is divided into amide, spacer, and norbornyl parts. A summary of interactions and modifications lowering the potency of the compound is indicated.

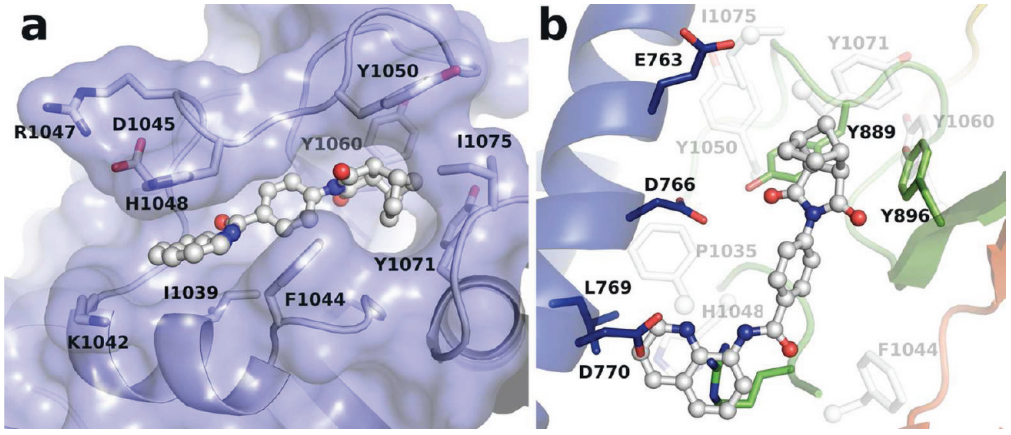

Figure 5. Specificity and selectivity of **2** for tankyrases. (a) Surface representation of the binding cavity induced by **2** binding to TNKS2. The compound is shown as sticks, and the molecular surface of TNKS2 is shown in blue. The residues lining the cavity are shown as sticks. (b) A comparison of **2**–TNKS2 complex and PARP1 structure (PDB code 2RD6[33]). Residues potentially interacting and clashing with **2** in the case of PARP1 are shown, and the structure is colored as in Figure 1a. Selected residues surrounding **2** in tankyrase are shown as transparent sticks.

Tyr1050 and Tyr1060, and one at the amide part with the backbone amide of Asp1045 (Figure 3c). The norbornyl region binds in the middle of a triangle formed by three tyrosines, Tyr1050, Tyr1060, and Tyr1071, all adopting a conformation distinct from the other crystal structures. The Tyr1050 of the D-loop has moved, on average, 5 Å away from the cleft, to form nonpolar interactions with **2** and Ile1075. The side chain of Tyr1060 has moved 1 Å closer to **2**, and Tyr1071 has rotated 51° to interact with the compound. This rotation closes the nicotinamide-binding site and would prevent binding of the nicotinamide to the now smaller cavity. The catalytic Glu1138 has adopted a conformation slightly different from that when nicotinamide and **1** are bound. The spacer region of **2** is located between the reorganized D-loop and the mostly hydrophobic region formed by His1031, Phe1044, and Ile1059. The quinoline moiety of the amide part is located between the hydrophobic face of the helix 1035–1042 and His1048, which would completely overlap with the amide region if it were not to move out of the cavity.

Structure–Activity Relationship of IWR-1 Analogues. Before the molecular target of **2** was known, a structure–activity study was reported, analyzing different modifications to the basic structure.[24] Although this was conducted in a cell-based assay, the crystal structure gives explanations to some of the effects. Modifications of **2** at different parts (Figure 4) suggested that all three regions are critical for the potency of the inhibitor, as all changes made the compound less potent. In the structure of the complex, His1048 shows a large movement, which, together with rotation of Phe1035, creates a new cavity in the protein where the quinoline binds (Figure 5a). The quinoline ring was found to be critical for the potency, and substitution with other groups led to loss of activity.[24] Substitution of quinoline with smaller aromatic phenyl, benzyl, or pyridyl groups made the compound almost inactive (EC_{50} > 20 μM). This highlights the importance of this region for the potency of the compound. The quinoline bicycle is large enough to drive the opening of the D-loop, and it effectively fills the resulting cavity (Figure 5a). Phenyl derivatives substituted with halogen at position 4 improved the potency to the micromolar range ($EC_{50} \approx 2.6$ μM); the 4-pyridyl-(methyl) derivative also showed somewhat improved potency ($EC_{50} = 10$ μM) over the pyridyl derivative. These substitutions at the para-position could create new interactions with Lys1042 at the end of the binding groove, explaining the improved potency (Figure 3c). As the binding site does not contain candidates for aromatic stacking interactions, other than to His1048, it is also possible to have a nonaromatic amide group with a reasonable potency. This was true for *trans*-(2-methoxy)cyclohexyl derivative showing $EC_{50} = 2$ μM. The potency is probably improved through hydrophobic inter-

dx.doi.org/10.1021/jm201510p | J. Med. Chem. 2012, 55, 1360–1367

actions with the α-helix 1035−1042, similar to what was observed for **1** (Figure 3b and Figure 3c). It also explains the reasonable potency of the 2-methoxyphenyl analogue (1 μM). Importantly, the *N*-methyl derivative of **2** was completely inactive (Figure 4).[24] The reason is that this modification restricts the conformation of the compound so that it cannot adopt the conformation observed in the crystal structure.

The central aromatic spacer region forms hydrophobic interactions with the surrounding side chains (Figure 3c). The aromaticity of the spacer is not important, as a saturated analogue showed only a 2-fold drop in potency.[24] One highly important feature of this spacer is its length, as addition of only one atom between amide and norbornyl regions completely abolished the activity. At the norbornyl region, there is no room to move toward the nicotinamide site, and it would not be favorable to push the amide region out from the hydrophobic pocket toward the solvent and charged residues (Lys1042, Asp1045, Arg1047, and His1048) at the delta of the cleft. Small substituents at position 3 of the spacer (Figure 4) are tolerated, whereas substituents at position 2 abolish the activity. At position 3 there would be more room, especially on the side of the flexible D-loop (Figure 5a).

Exo-IWR-1 showed 25-fold lower potency than endo-IWR-1 **2**, whereas a saturated norbornane had similar potency to **2**.[16] On the basis of the crystal structure, the saturated analogue would fit into the cavity equally as well as **2**. Although binding of **2** causes changes in the Tyr1071, the exo-IWR-1 probably causes too much disturbance for the nicotinamide-binding site, explaining the 10-fold lower potency. It would also be less complementary to the observed binding cavity (Figure 5a).

Structural Explanation for Selectivity. Compound **2** is very selective toward tankyrases (IC_{50}(TNKS1) = 131 nM, IC_{50}(TNKS2) = 56 nM), compared to PARP1 and PARP2 (IC_{50} > 18.7 μM).[16] In comparison, **3** is approximately 10-fold selective toward tankyrases over PARP2. In order to confirm the low potency of **2**, we tested its effect on PARP1 and PARP2 using an activity-based assay.[25] This indicated that the IC_{50} would be approximately 100 and 35 μM, respectively (Supplementary Figure 1). This makes **2** at least 600-fold selective for tankyrases over both PARP1 and PARP2, which is significantly better than the selectivity reported for **3**.

Superposition of PARP1 on the TNKS2 complex with **2** revealed that some of the interactions with the proteins would be potentially similar, but it also clearly explains the remarkable selectivity of the compound. Amino acids Tyr896 and Asp766 of PARP1 correspond to Tyr1060 and Asp1045 of TNKS2 that form hydrogen bonds with **2** (Figures 3c and 5b). Tyr889 could partly replace the third hydrogen bond formed between **2** and Tyr1050 of TNKS2. Two of the three tyrosines surrounding the norbornyl region are conserved in PARP1, as Tyr1050 could be potentially replaced by Tyr889 of the PARP1 D-loop. Ile1075 and the following zinc-binding motif are not present in PARP1, and a negatively charged side chain of Glu763 of the PRD domain is located at this position (Figure 5b). Asp766 of the PARP1 PRD domain could form a hydrogen bond with the norbornyl carbonyl, but it would require protonation of the aspartate.

At the quinoline-binding site, there are larger differences between the structures. Phenylalanines 1035 and 1044 surrounding the spacer and amide regions are not conserved in PARP1. The α-helix lining the binding site is of more polar nature in PARP1, and Phe1035 is completely missing. Also, the stacking of His1048 with quinoline is not conserved in TNKS2. The quinoline severely clashes with the salt bridge formed by Arg878 and Asp770 of PARP1 PRD (Figure 5b). The reorganization of the salt bridge is possible, as binding of **1** would cause this change and different conformations of PARP1 Arg878 have been observed in crystal structures.[19] The clashes with **2** and the PARP1 regulatory region would require a large movement of the PARP1 domains with respect to each other. These selective features of **2** make it a good model especially for the development of inhibitors of tankyrases.

■ DISCUSSION AND CONCLUSIONS

Experimental structures can reveal important interactions with lead inhibitors that can be utilized in structure-based design to improve existing inhibitors and to discover new ones. Increasing evidence supports the therapeutic potential of targeting tankyrase, and we have used protein crystallography to study the binding of inhibitors to TNKS2. We describe here crystal structures of the product of cleavage of NAD^+, nicotinamide, and inhibitors **1** and **2** bound to TNKS2. So far, no complex of any of the PARP isoenzymes with a substrate exists in the Protein Data Bank and not even a hydrolyzed product complex has been available. We observed a nicotinamide complex in NAD^+-soaked crystals of TNKS2, confirming the expected binding site that has been utilized for decades in the design of inhibitors. It indicated that the chymotrypsin-cleaved protein would be active, which was also confirmed by using a biotinylated substrate. This also provides support that the crystal form of the catalytic ART domain, which can accommodate inhibitors without destroying crystal packing, represents the biological molecule reasonably well and will thus be useful for drug discovery efforts. The cleavage probably affects the affinity of the target proteins toward the acceptor binding site, but it does not directly affect the donor site utilized by the known PARP inhibitors.

The structure of the complex of TNKS2 with a PARP-selective inhibitor **1** revealed interactions that could be mostly conserved in PARP1 and PARP2. Structures of **1** complexed with PARP have not previously been available, but a structure of an analogue, KU0058948, has been solved in complex with human PARP3.[22] The structures show that the binding mode in PARP1−3 is different from the one seen in TNKS2. The fluorophenyl is stacking with another tyrosine, and the selectivity of **1** for PARP1−3 over tankyrases comes from the interactions with the variable D-loop lining the donor site (Supplementary Figure 2). A hydrogen bond of the fluorophenyl group with an H-bond donor would be more favorable than interactions with the carbonyl groups in TNKS2.[26] The binding of **1** induced opening of the D-loop in TNKS2, which has shown a closed conformation in previously solved TNKS1 and TNKS2 structures.[21,22] This open structure probably closely resembles the substrate-bound form, as binding of NAD^+ would also require such an opening of the structure.

Inhibitor **2** does not utilize the nicotinamide-binding site used by most of the other inhibitors of PARPs.[27] Binding of **2** induces changes in the structure, affecting also the nicotinamide-binding site, but most importantly it causes opening of the D-loop. Induced fit makes **2** highly complementary to the new cavity. This change is very specific, as modification of the different regions of the compound led to lower potency or completely abolished the activity of the compound. It highlights that all three regions, i.e., amide, spacer, and norbornyl, are required for potency through specific

Table 1. Data Collection and Refinement Statistics[a]

	1	2	nicotinamide (NAD^+)
	Data Collection		
space group	$P4_12_12$	$C222_1$	$C222_1$
cell dimensions			
a, *b*, *c* (Å)	66.50, 66.50, 115.92	92.81, 93.70, 121.96	91.25, 97.75, 119.16
α, β, γ (deg)	90, 90, 90	90, 90, 90	90, 90 90
resolution (Å)	50−2.3 (2.36−2.30)	50−2.15 (2.21−2.15)	50−1.75 (1.80−1.75)
R_{merge}	0.113 (0.601)	0.043 (0.393)	0.068 (0.691)
$I/\sigma I$	16.41 (3.39)	16.86 (2.18)	18.69 (3.05)
completeness (%)	100 (100)	99.3 (96.5)	100 (100)
redundancy	7.0 (7.2)	3.3 (2.2)	7.2 (7.3)
	Refinement		
resolution (Å)	50−2.3	50−2.15	50−1.75
no. reflections	11182	27621	51211
R_{work}/R_{free}	0.181/0.233	0.205/0.239	0.166/0.197
no. atoms			
protein	1680	3331	3394
ligand/ion	49	98	65
water	138	86	362
B-factor			
protein	20.7	35.2	21.7
ligand/ion	33.1	45.6	33.2
water	27.0	31.2	30.2
rms deviation			
bond length (Å)	0.014	0.015	0.008
bond angle (deg)	1.398	1.462	1.564

[a]Values in parentheses are for highest-resolution shell.

interactions and by separating the different pharmacophoric features by the correct distances. When the TNKS2 complex is compared with the structure of PARP1, it is found that there are evident clashes of PARP1 residues and **2**. Some of the interactions at the norbornyl region are conserved or contain complementary interactions. There are severe clashes between the α-helical PRD domain of PARP1 and **2**, indicating that the PARP1 domains need to open in order to accommodate **2**. While the D-loop of PARP1 could move to accommodate the inhibitor, the required movement of domains and missing interactions in PARP1 explain the remarkable selectivity of the compound toward the tankyrases.

The structure of the complex of TNKS2 and **2** can be used for the design of selective inihibitors of tankyrase. The unique interactions between TNKS2 and **2** define a new pharmacophore model. As the structure represents the first elucidated complex with an inhibitor not binding to the nicotinamide-binding site, it could also provide new ideas for development of inhibitors of PARPs in general. Clearly, the plasticity of the D-loop should be recognized when designing inhibitors for PARPs lacking the regulatory domain.

EXPERIMENTAL SECTION

Tested Compounds. Purity of all the tested compounds was measured by the suppliers using HPLC. All the compound batches had >95% purity.

Protein Expression and Purification. An expression construct for the catalytic ART domain of human TNKS2 (residues 952−1161) was a generous gift from Structural Genomics Consortium (Stockholm, Sweden). The plasmid pNIC-Bsa4 contained N-terminal hexahistidine tag MHHHHHHSSGVDLGTENLYFQSM before TEV-cleavage site. Plasmid was transferred to *E. coli* BL21 (DE3) Rosetta2 cells. Overnight preculture (5 mL) in Terrific Broth (TB) medium containing 34 μg/mL chloramphenicol and 50 μg/mL kanamycin was used to inoculate 4 × 750 mL of autoinduction TB medium containing trace elements (ForMedium) with 8 g/L glycerol, 34 μg/mL chloramphenicol, and 50 μg/mL kanamycin. Cultures were incubated at 37 °C/180 rpm in shake flasks until the turbidity of the culture, i.e., OD_{600}, reached 1. The temperature was then lowered to 18 °C. Incubation was continued overnight, and after 15 h, cells were harvested by centrifugation (4 °C, 5500*g*, 10 min). The pellet was resuspended in lysis buffer (100 mM HEPES, pH 7.5, 500 mM NaCl, 10% glycerol, 10 mM imidazole, and 0.5 mM TCEP), and the solution was stored at −20 °C.

The cell suspension was quickly thawed in warm water, and 2 mM TCEP, approximately 0.2 mg of lysozyme, 250 U of benzonase (Sigma-Aldrich), and an EDTA-free protease inhibitor tablet (Roche) were added. The cells were disrupted by sonicating the cell suspension on an ice−water bath for 10 min with a 50% duty cycle (Branson 250 sonifier). The solution was cleared by centrifugation (4 °C, 35000*g*, 20 min), and the supernatant was filtered through 0.45 μm filters. The sample was loaded on a HisTrap HP column (GE Healthcare), which had been pre-equilibrated with binding buffer at 4 °C (30 mM HEPES, pH 7.5, 500 mM NaCl, 10% (w/v) glycerol, 10 mM imidazole, 0.5 mM TCEP), and the column was washed with the same buffer. Purification was further performed with Äkta purifier (GE Healthcare) at room temperature. The column was washed with buffer containing 25 mM imidazole, and elution was carried out with buffer containing 250 mM imidazole while collecting 0.25 mL fractions. The pooled fractions were loaded on a size-exclusion column (Hiprep 16/60 Sepharyl S-100 HR; GE Healthcare), pre-equilibrated with gel filtration buffer (30 mM HEPES, pH 7.5, 500 NaCl, 10% w/v glycerol, 0.5 mM TCEP). The fractions were analyzed with SDS−PAGE electrophoresis, and the protein was concentrated using Vivaspin 20 concentrators (Sartorius Stedim Biotech). Precipitation of the protein was observed during the concentration, so chymotrypsin (100 nM) was added as reported in the previous structural studies.[21] The concentration of the protein (5.5 mg/mL) was measured using the extinction coefficient calculated from the sequence and the absorbance at 280 nm. For the intact protein preparation, the protein was cleaved with TEV protease[28] overnight at +4 °C and passed through a HisTrap

dx.doi.org/10.1021/jm201510p | J. Med. Chem. 2012, 55, 1360−1367

HP column before concentration to 2.7 mg/mL. The protein preparations were flash-frozen in liquid nitrogen and stored at −70 °C in small aliquots.

Activity Assay. A Western blot based activity assay was performed on the purified tankyrase catalytic domains. Enzymatic reaction contained only protein (1 μM) and 10 μM biotinylated NAD^+ (Trevigen), which is a substrate modified with biotin. The reaction was carried out in buffer containing 50 mM Bis-Tris propane at pH 7.0 and 0.5 mM TCEP. The mixture was incubated for 3 h at 25 °C with shaking at 300 rpm. The reaction mixture was run on an SDS−PAGE electrophoresis gel (Bio-Rad), and the proteins on a gel were transferred and immobilized onto a nitrocellulose membrane by the semidry transfer method. To avoid background signal, the membrane was blocked by placing it for 12 h to Tris-buffered saline supplemented with 0.1% Tween-20 and 1% casein. Streptavidin-HRP (PerkinElmer) was diluted 20000-fold with 1% casein in Tris-buffered saline, and the membrane was incubated in this solution for 90 min. The automodification activity of the proteins was monitored by detecting luminescence on a film using horseradish proxidase substrate solution (Western Lightning PLUS; PerkinElmer). This identifies proteins that are covalently modified with biotinylated ADP-ribose.

Crystallization. Crystals were obtained using sitting-drop vapor-diffusion method in a 96-well plate. An amount of 0.1 μL of protein solution (5.5 mg/mL) was mixed with 0.2 μL of well solution consisting of 0.2 M Li_2SO_4, 0.1 M Tris-HCl, pH 8.5, and 22−26% PEG 3350. The plate was incubated at 4 °C, and crystals grew within 1 week. The crystals were soaked in the solution (0.1 M Tris, pH 8.5, 0.2 M Li_2SO_4, 250 mM NaCl, and 22% PEG 3350) supplemented with 100 μM **2** (Sigma-Aldrich), 100 μM **1** (JS Research Chemicals Trading), or 10 mM NAD^+ (Sigma-Aldrich) for 24 h. Crystals were picked up with a loop, dipped into a cryosolution (0.1 M Tris, pH 8.5, 0.2 M Li_2SO_4, 250 mM NaCl and 22% PEG 3350, 22% glycerol, 100 μM inhibitor or 10 mM NAD^+) and flash frozen in liquid nitrogen.

Data Collection and Refinement. Diffraction data were collected to 2.15 Å (**2**), 2.3 Å (**1**), and 1.75 Å (NAD^+) at the synchrotron, and the data were processed with XDS.[29] The crystals belonged to space group $C222_1$ or to space group $P4_12_12$ (Table 1). The structures were solved by molecular replacement using the apo-TNKS2 structure (PDB code 3KR7) as a model. The refinement was achieved using Refmac5[30] from the CCP4 program suite,[31] and Coot[32] was used for manual editing.

Structure Analysis and Visualization. Pymol (Schrödinger) was used for constructing the structure figures, and Coot[32] was used for superpositions and analysis of the structure, together with tools of the CCP4 program suite.[31]

■ ASSOCIATED CONTENT

Ⓢ Supporting Information

A figure showing the affect of **2** with human PARP1 and PARP2, a description of the method, and a figure showing comparison of **1** binding to TNKS2 and PARP3. This material is available free of charge via the Internet at http://pubs.acs.org.

Accession Codes

†Coordinates and structure factors are deposited at the Protein Data Bank with codes 3U9H, 3U9Y, and 3UA9.

■ AUTHOR INFORMATION

Corresponding Author

*Phone: +358 2 2157420. E-mail: lari.lehtio@oulu.fi.

■ ACKNOWLEDGMENTS

The work was supported by funding from the Academy of Finland (Grant No. 128322) and from Sigrid Jusélius foundation. M.N. and H.V. are members of the National Doctoral Programme of Informational and Structural Biology. We are grateful to local contacts at ESRF for providing assistance in using beamlines ID23-1 and ID14-1.

■ ABBREVIATIONS USED

ART, ADP-ribosyltransferase; BRCA, breast cancer; NAD^+, nicotinamide adenine dinucleotide; pADPr, poly(ADP-ribose); PARP, poly(ADP-ribose) polymerase; SAM, sterile α motif; TKNS, tankyrase; TRF, telomere repeat binding factor

■ REFERENCES

(1) Hakmé, A.; Wong, H. K.; Dantzer, F.; Schreiber, V. The expanding field of poly(ADP-ribosyl)ation reactions. *EMBO Rep.* **2008**, *9*, 1094−1100 ("Protein Modifications: Beyondthe Usual Suspects" Review Series).

(2) Hottiger, M. O.; Hassa, P. O.; Lüscher, B.; Schüler, H.; Koch-Nolte, F. Toward a unified nomenclature for mammalian ADP-ribosyltransferases. *Trends Biochem. Sci.* **2010**, *35*, 208−219.

(3) De Rycker, M.; Price, C. M. Tankyrase polymerization is controlled by its sterile alpha motif and poly(ADP-ribose) polymerase domains. *Mol. Cell. Ther.* **2004**, *24*, 9802−9812.

(4) Chiang, Y. J.; Hsiao, S. J.; Yver, D.; Cushman, S. W.; Tessarollo, L.; Smith, S.; Hodes, R. J. Tankyrase 1 and tankyrase 2 are essential but redundant for mouse embryonic development. *PLoS One* **2008**, *3*, e2639.

(5) Hsiao, S. J.; Smith, S. Tankyrase function at telomeres, spindle poles, and beyond. *Biochimie* **2008**, *90*, 83−92.

(6) Chang, P.; Coughlin, M.; Mitchison, T. J. Tankyrase-1 polymerization of poly(ADP-ribose) is required for spindle structure and function. *Nat. Cell Biol.* **2005**, *7*, 1133−1139.

(7) Chang, P.; Jacobson, M. K.; Mitchison, T. J. Poly(ADP-ribose) is required for spindle assembly and structure. *Nature* **2004**, *432*, 645−649.

(8) McCabe, N.; Cerone, M. A.; Ohishi, T.; Seimiya, H.; Lord, C. J.; Ashworth, A. Targeting tankyrase 1 as a therapeutic strategy for BRCA-associated cancer. *Oncogene* **2009**, *28*, 1465−1470.

(9) Counter, C. M.; Botelho, F. M.; Wang, P.; Harley, C. B.; Bacchetti, S. Stabilization of short telomeres and telomerase activity accompany immortalization of Epstein−Barr virus-transformed human B lymphocytes. *J. Virol.* **1994**, *68*, 3410−3414.

(10) Counter, C. M.; Avilion, A. A.; LeFeuvre, C. E.; Stewart, N. G.; Greider, C. W.; Harley, C. B.; Bacchetti, S. Telomere shortening associated with chromosome instability is arrested in immortal cells which express telomerase activity. *EMBO J.* **1992**, *11*, 1921−1929.

(11) Folini, M.; Gandellini, P.; Zaffaroni, N. Targeting the telosome: therapeutic implications. *Biochim. Biophys. Acta* **2009**, *1792*, 309−316.

(12) Smith, S.; de Lange, T. Tankyrase promotes telomere elongation in human cells. *Curr. Biol.* **2000**, *10*, 1299−1302.

(13) Seimiya, H.; Muramatsu, Y.; Ohishi, T.; Tsuruo, T. Tankyrase 1 as a target for telomere-directed molecular cancer therapeutics. *Cancer Cell* **2005**, *7*, 25−37.

(14) Polakis, P. The many ways of Wnt in cancer. *Curr. Opin. Genet. Dev.* **2007**, *17*, 45−51.

(15) Barker, N.; Clevers, H. Mining the Wnt pathway for cancer therapeutics. *Nat. Rev. Drug Discovery* **2006**, *5*, 997−1014.

(16) Huang, S.-M. A.; Mishina, Y. M.; Liu, S.; Cheung, A.; Stegmeier, F.; Michaud, G. A.; Charlat, O.; Wiellette, E.; Zhang, Y.; Wiessner, S.; Hild, M.; Shi, X.; Wilson, C. J.; Mickanin, C.; Myer, V.; Fazal, A.; Tomlinson, R.; Serluca, F.; Shao, W.; Cheng, H.; Shultz, M.; Rau, C.; Schirle, M.; Schlegl, J.; Ghidelli, S.; Fawell, S.; Lu, C.; Curtis, D.; Kirschner, M. W.; Lengauer, C.; Finan, P. M.; Tallarico, J. A.; Bouwmeester, T.; Porter, J. A.; Bauer, A.; Cong, F. Tankyrase inhibition stabilizes axin and antagonizes Wnt signalling. *Nature* **2009**, *461*, 614−620.

(17) Chen, B.; Dodge, M. E.; Tang, W.; Lu, J.; Ma, Z.; Fan, C.-W.; Wei, S.; Hao, W.; Kilgore, J.; Williams, N. S.; Roth, M. G.; Amatruda, J. F.; Chen, C.; Lum, L. Small molecule-mediated disruption of Wnt-dependent signaling in tissue regeneration and cancer. *Nat. Chem. Biol.* **2009**, *5*, 100−107.

(18) Menear, K. A.; Adcock, C.; Boulter, R.; Cockcroft, X.-ling; Copsey, L.; Cranston, A.; Dillon, K. J.; Drzewiecki, J.; Garman, S.; Gomez, S.; Javaid, H.; Kerrigan, F.; Knights, C.; Lau, A.; Loh, V. M.;

Matthews, I. T. W.; Moore, S.; O'Connor, M. J.; Smith, G. C. M.; Martin, N. M. B. 4-[3-(4-Cyclopropanecarbonylpiperazine-1-carbonyl)-4-fluorobenzyl]-2*H*-phthalazin-1-one: a novel bioavailable inhibitor of poly(ADP-ribose) polymerase-1. *J. Med. Chem.* **2008**, *51*, 6581−6591.

(19) Ruf, A.; de Murcia, G.; Schulz, G. E. Inhibitor and NAD^+ binding to poly(ADP-ribose) polymerase as derived from crystal structures and homology modeling. *Biochemistry* **1998**, *37*, 3893−3900.

(20) Miranda, E. A.; Dantzer, F.; O'Farrell, M.; de Murcia, G.; de Murcia, J. M. Characterisation of a gain-of-function mutant of poly(ADP-ribose) polymerase. *Biochem. Biophys. Res. Commun.* **1995**, *212*, 317−325.

(21) Karlberg, T.; Markova, N.; Johansson, I.; Hammarström, M.; Schütz, P.; Weigelt, J.; Schüler, H. Structural basis for the interaction between tankyrase-2 and a potent Wnt-signaling inhibitor. *J. Med. Chem.* **2010**, *53*, 5352−5355.

(22) Lehtiö, L.; Collins, R.; van den Berg, S.; Johansson, A.; Dahlgren, L.-G.; Hammarström, M.; Helleday, T.; Holmberg-Schiavone, L.; Karlberg, T.; Weigelt, J. Zinc binding catalytic domain of human tankyrase 1. *J. Mol. Biol.* **2008**, *379*, 136−145.

(23) Gelmon, K. A.; Tischkowitz, M.; Mackay, H.; Swenerton, K.; Robidoux, A.; Tonkin, K.; Hirte, H.; Huntsman, D.; Clemons, M.; Gilks, B.; Yerushalmi, R.; Macpherson, E.; Carmichael, J.; Oza, A. Olaparib in patients with recurrent high-grade serous or poorly differentiated ovarian carcinoma or triple-negative breast cancer: a phase 2, multicentre, open-label, non-randomised study. *Lancet Oncol.* **2011**, *12*, 852−861.

(24) Lu, J.; Ma, Z.; Hsieh, J.-C.; Fan, C.-W.; Chen, B.; Longgood, J. C.; Williams, N. S.; Amatruda, J. F.; Lum, L.; Chen, C. Structure−activity relationship studies of small-molecule inhibitors of Wnt response. *Bioorg. Med. Chem. Lett.* **2009**, *19*, 3825−3827.

(25) Putt, K. S.; Hergenrother, P. J. An enzymatic assay for poly(ADP-ribose) polymerase-1 (PARP-1) via the chemical quantitation of NAD(+): application to the high-throughput screening of small molecules as potential inhibitors. *Anal. Biochem.* **2004**, *326*, 78−86.

(26) Auffinger, P.; Hays, F. A.; Westhof, E.; Ho, P. S. Halogen bonds in biological molecules. *Proc. Natl. Acad. Sci. U.S.A.* **2004**, *101*, 16789−16794.

(27) Ferraris, D. V. Evolution of poly(ADP-ribose) polymerase-1 (PARP-1) inhibitors. From concept to clinic. *J. Med. Chem.* **2010**, *53*, 4561−4584.

(28) van den Berg, S.; Löfdahl, P.-A.; Härd, T.; Berglund, H. Improved solubility of TEV protease by directed evolution. *J. Biotechnol.* **2006**, *121*, 291−298.

(29) Kabsch, W. Automatic processing of rotation diffraction data from crystals of initially unknown symmetry and cell constants. *J. Appl. Crystallogr.* **1993**, *26*, 795−800.

(30) Murshudov, G. N.; Vagin, A. A.; Dodson, E. J. Refinement of macromolecular structures by the maximum-likelihood method. *Acta Crystallogr., Sect. D: Biol. Crystallogr.* **1997**, *D53*, 240−255.

(31) Dodson, E. J.; Winn, M.; Ralph, A. Collaborative computational project, number 4: providing programs for protein crystallography. *Methods Enzymol.* **1997**, *277*, 620−633.

(32) Emsley, P.; Cowtan, K. Coot: model-building tools for molecular graphics. *Acta Crystallogr., Sect. D: Biol. Crystallogr.* **2004**, *D60*, 2126−2132.

(33) Penning, T. D.; Zhu, G.-D.; Gandhi, V. B.; Gong, J.; Liu, X.; Shi, Y.; Klinghofer, V.; Johnson, E. F.; Donawho, C. K.; Frost, D. J.; Bontcheva-Diaz, V.; Bouska, J. J.; Osterling, D. J.; Olson, A. M.; Marsh, K. C.; Luo, Y.; Giranda, V. L. Discovery of the poly(ADP-ribose) polymerase (PARP) inhibitor 2-[(*R*)-2-methylpyrrolidin-2-yl]-1*H*-benzimidazole-4-carboxamide (ABT-888) for the treatment of cancer. *J. Med. Chem.* **2009**, *52*, 514−523.